Journal of Molecular Catalysis A: Chemical 348 (2011) 106–113

Contents lists available at SciVerse ScienceDirect

Journal of Molecular Catalysis A: Chemical

journal homepage: www.elsevier.com/locate/molcata

Preparation, characterization and catalytic performance of the silica pillared clay incorporated with phosphotungstic acid using different surfactants as template

Baoshan Li[a,*], Zhenxing Liu[a], Chunying Han[a], Jianjun Liu[a], Shengli Zuo[a], Zhiyuan Zhou[b], Xinmei Pang[b]

[a] State Key Laboratory of Chemical Resource Engineering, Beijing University of Chemical Technology, Beijing 100029, PR China
[b] Petrochina Petrochemical Research Institute, Beijing 100029, PR China

ARTICLE INFO

Article history:
Received 2 April 2011
Received in revised form 14 August 2011
Accepted 16 August 2011
Available online 24 August 2011

Keywords:
Silica pillared clay
Montmorillonite
Tungstophosphoric acid
Catalytic oxidative desulfurization

ABSTRACT

The mesoporous silica pillared clay (SPC) incorporated with Keggin-type $H_3PW_{12}O_{40}$ (HPW) heteropoly acid was prepared by introducing HPW into clay interlayer template in an acidic suspension using sol–gel method. The materials are readily separable mesoporous materials with high specific surface areas. The results indicate that the surfactants play a decisive role in the introduction of HPW molecule and the pore formation. Moreover, the surface area and pore size of the materials can be controlled by the molecular length and functional groups of the surfactants. The formation mechanism of the materials was also proposed. The synthesized materials exhibited good catalytic performance in oxidative desulfurization of dibenzothiophene-containing model oil. Under the best conditions, the sulfur removal can reach up to near 100%. The excellent catalytic performance for oxidative desulfurization opens up new opportunities for applications of the synthesized materials in catalysis.

1. Introduction

It has been an urgent subject to find new processes for ultra-deep desulfurization of fuel oils because of the increasing environmental concern and legal requirements. However, the conventional hydrodesulfurization (HDS) technique has difficulty in reducing refractory sulfur-containing compounds such as dibenzothiophene (DBT) and its derivatives to an ultra low level. Thus, a large number of non-HDS processes such as adsorption, extraction, oxidation, precipitation and bio-processes have been explored [1–5]. Among these methods, catalytic oxidative desulfurization (ODS) combined with extraction is regarded as the most promising and economical process [6,7]. Polyoxometalates (POMs) have been widely used as oxidation catalysts in treating sulfur-containing compounds in a liquid–liquid two-phase system due to their excellent physical and chemical properties. However, the catalytic activities of the POMs are greatly limited by their very low specific surface areas [8]. Moreover, they are soluble in aqueous solution and not easily separated from the reaction system for recycling use. Therefore, many attempts have been made to enhance the catalytic activity and obtain sustainable catalytic performance of the POMs [9,10].

On the other hand, inorganic porous materials with a controlled pore structure have stimulated a great deal of interest for their potential application as selective catalysts, adsorbents, separating agents, and porous matrixes for encapsulation of specific functional molecules [11–13]. In our previous work, monovacant lacunary Keggin-type polyoxometalate was introduced into mesoporous silica structure and showed high oxidation activity for ODS [14]. Furthermore, a series of ordered mesoporous clay materials known as silica pillared clay (SPC) materials and metal ion doped SPC materials have been recently prepared [15–25].

In the present work, in order to combine the porous advantages of SPC and the appropriate acidity of $H_3PW_{12}O_{40}$ (HPW) heteropoly acid, we encapsulated HPW into the ordered mesoporous SPC materials by sol–gel method. The products were denoted as HPW-SPC. The influence of the surfactants on the structure and properties of the HPW-SPC materials was studied. The catalytic performance of the samples was examined through the ODS of the DBT-containing model oil. The results indicate that the HPW-SPC materials exhibited a high catalytic activity in ODS of DBT.

2. Experimental

2.1. Materials

All solvents and reactants are commercially available and were used without further purification. The natural montmorillonite clay (MMT) was obtained from Inner Mongolia and used as the starting clay without any further purification or cations exchanging. The raw clay had a basal (001) spacing of 15.4 Å and an anhydrous structural (layer) formula of

* Corresponding author. Tel.: +86 106 444 5611; fax: +86 106 444 5611.
E-mail address: bsli@mail.buct.edu.cn (B. Li).

1381-1169/$ – see front matter © 2011 Elsevier B.V. All rights reserved.
doi:10.1016/j.molcata.2011.08.014

Table 1
The results of the XRF analysis of the samples.

Catalyst composition		HPW-SPC-4	HPW-SPC-12	HPW-SPC-16	HPW-SPC-18
Before reaction	P_2O_5/wt.%	0.32	0.31	0.32	0.34
	WO_3/wt.%	12.7	13.1	12.8	13.7
	P:W:Si:Al	1:12.1:288.9:32.4	1:12.8:293.2:7.2	1:12.3:288.9:21.4	1:12.3:272.9:14.6
	HPW/wt.%	13.1	13.5	13.2	14.2
After the fourth recycle reaction	P_2O_5/wt.%	–	0.17	0.22	0.12
	WO_3/wt.%	–	6.44	8.30	4.59
	P:W:Si:Al	–	1:11.6:428.8:22.0	1:11.5:388.7:30.2	1:11.3:794.3:84.0
	HPW/wt.%	–	6.66	8.59	4.75

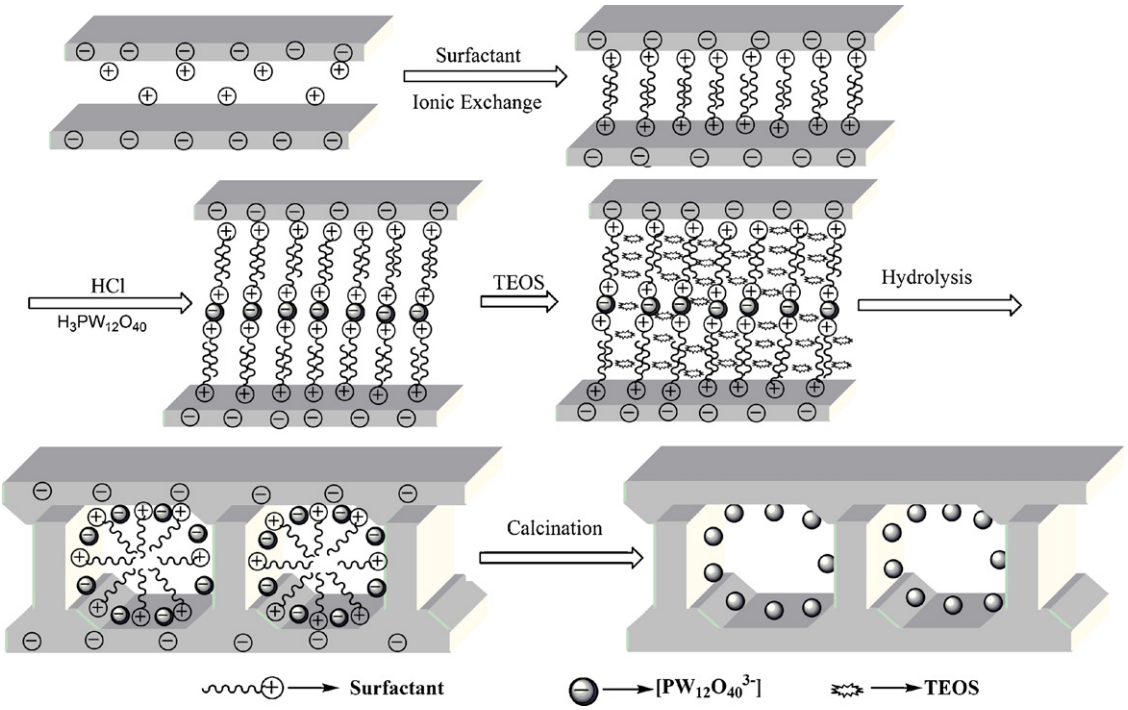

Scheme 1. Formation mechanism of the HPW-SPC samples.

$Ca_{0.48}Na_{0.03}K_{0.01}[Si_{7.86}Al_{0.14}][Al_{2.84}Fe_{0.30}Mg_{0.86}]O_{20}(OH)_4$, with a cation exchange capacity (CEC) of 91 meq/100 g [15]. Octadecyl dimethyl benzyl ammonium chloride (C_{18}DMBACl) and dodecyl dimethylbenzyl ammonium chloride (C_{12}DMBACl) were synthesized based on a previously reported procedure [19].

2.2. Preparation

A given amount of MMT was suspended in 120 mL of deionized water in a round bottom flask, to which the ethanol solution of C_{18}DMBACl was added dropwise and stirred for 1 h and a gel mixture was gained. Then, the pH of the gel was adjusted by HCl aqueous solution to 2.0. Subsequently, a given amount of $H_3PW_{12}O_{40}{\cdot}5H_2O$ was dissolved in water, and added dropwise into the gel under vigorous stirring. After the mixture was stirred for 4 h, tetraethyl orthosilicate (TEOS) was added, followed by stirring for 12 h at room temperature. The molar ratio of clay, C_{18}DMBACl, TEOS, ethanol and water was 1/0.4/1.6/6.3/258 [24]. The addition content of HPW was supposed to be 15 wt.% in the sample (the actual content obtained by XRF was list in Table 1). And then, the mixture was put into an autoclave and heated for 24 h at 110 °C. Afterward, the autoclave was cooled, and the product was separated by filtration, throughly washed with deionized water, and dried in an oven at 110 °C. Finally, the dried sample was calcined at 400 °C for 6 h in a furnace. The sample was designated as HPW-SPC-18.

The HPW-SPC-4, HPW-SPC-12, and HPW-SPC-16 samples were prepared following the same procedure as the HPW-SPC-18 sample, but the surfactants were changed into tetrabutylammonium bromide (TBAB), C_{12}DMBACl, and cetyltrimethylammonium bromide (CTAB), respectively.

The SPC samples were also prepared following the same procedure as the HPW-SPC samples but without addition of HPW. The samples were designated as SPC-4, SPC-12, SPC-16, and

Table 2
The textural properties of the MMT and HPW-SPC samples.

Catalysts	Pore size/nm	S_{BET}/m^2 g^{-1}	Basal spacing/nm	Gallery height/nm	V_T/cm^3 g^{-1}
MMT	4.3	80	1.54	0.58	0.13
HPW-SPC-4	3.8	162	1.98	1.02	0.41
HPW-SPC-12	7.2	474	4.22	3.26	1.09
HPW-SPC-16	4.5	377	4.43	3.47	0.64
HPW-SPC-18	9.0	433	4.80	3.84	1.29

SPC-18, which were prepared using TBAB, C_{12}DMBACl, CTAB, and C_{18}DMBACl as the surfactants, respectively.

2.3. Catalytic performance in oxidative desulphurization

The model compound DBT was dissolved into *n*-octane to make a stock solution of model oil with sulfur content of 500 ppm. The reaction was performed in a three-neck flask with a water-bathed jacket. A mixture of model oil (25 mL) and catalyst (0.15 g) was heated in the reactor under stirring. When the reaction temperature reached up to 60 °C, 0.12 mL of 30% aqueous solution of H_2O_2 ($n_{H_2O_2}/n_S = 3$) was added into the reactor and the reaction temperature was kept at 60 °C. After continuously stirring for a certain time, the oxidized model oil was extracted three times by acetonitrile. The volume ratio of the total solvent to model oil was 1:1. The amount of sulfur in the oil was determined by a Model WK-2D microcoulometric integrated analyzer (sulfur detection range from 0.2 to 5000 ppm, Jiangsu Jiang Fen Electroanalytical Instrument Co.).

2.4. Characterization of the samples

The X-ray diffraction (XRD) was performed on a Rigaku D/Max 2500 VBZ+/PC diffractometer using Cu-Kα radiation at low-angle range (2θ value 0.5–10°) and at wide-angle range (2θ value 3–70°). The X-ray fluorescence analysis (XRF) was performed on a Philips Magix-601 X-ray fluorescence spectrometer. The thermogravimetric and differential thermal analysis (TG–DTA) was carried out in air on a HCT-1 thermal analyzer (Hengjiu Kexue Co.) using a heating rate of 10 °C min^{-1}. The Nitrogen adsorption isotherms were obtained using a Micromeritics ASAP2020M instrument. The samples were degassed at 115 °C for 8 h before the measurement. The specific surface area (S_{BET}) was estimated by the BET equation, and the pore size distribution and the mesopore analysis were obtained from the desorption branch of the isotherm using the Barrett–Joyner–Halenda (BJH) method [18,26,27]. The scanning electron microscopy (SEM) micrographs were obtained on a Zeiss Supra 55 microscope operated at 30 kV. The FT-IR spectra were obtained in KBr pellets using a Bruker VECTOR 22 spectrometer in the range of 400–4000 cm^{-1}, and all spectra were collected at room temperature with a resolution of 4 cm^{-1}.

3. Results and discussion

3.1. The formation mechanism of the HPW-SPC samples

Scheme 1 illustrates the proposed formation mechanism of the HPW-SPC materials. Firstly, MMT was suspended in aqueous solutions and had an ion-exchange with surfactant. During this process, the surfactant formed micelle in the interlayer region. Then, the pH of the mixture gel was adjusted to 2.0 by using HCl aqueous solution and an appropriate amount of HPW was introduced. $PW_{12}O_{40}^{3-}$ can be attracted into the interlayer and substitute Br^- and Cl^- in the shell surrounding the micelle. Furthermore, the addition of HCl aqueous solution can keep the solution in a strong acidic environment to retain the Keggin-type HPW heteropoly acid intact. When TEOS was finally added into the gel mixture, it would intercalate into the clay interlayer region by solvation and rapidly hydrolyze in acidic condition to form the protonated $H_5SiO_4^+$ monomers. The silicate cations would interact with the anionic shell surrounding the surfactant micelle to trap both X^- (Cl^-, Br^-) and heteropoly anions, leading to the formation of a silica layer around the surfactant template. Thus, the heteropoly anions would be present at the interface between the silica and the surfactant micelle. During the long time stirring and the hydrothermal treatment of the gel, the silica layer was polymerized and formed the Si–O–Si bonds between the interlayer region. Washing and drying steps did not remove the heteropoly anions since they were trapped inside the clay interlayer. In the calcination step, the silica layer further condensed and yielded the completely cross-linked framework to strengthen the siloxane-pillars and the mesoporous structure, while the surfactant template decomposed and was eliminated from the pore system, but the HPW molecules remained fixed into the pore walls [26].

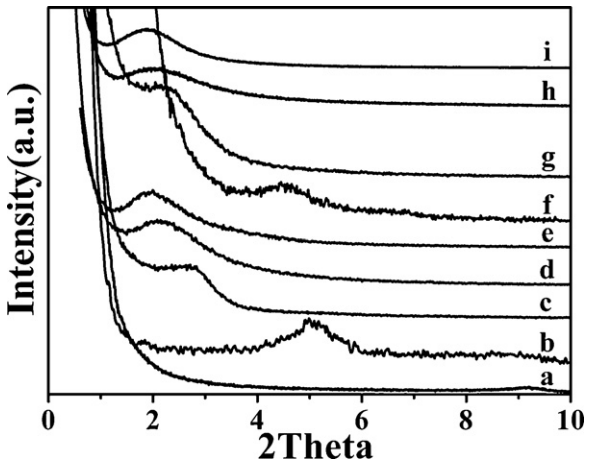

Fig. 1. The low-angle XRD patterns of the samples: (a) calcined MMT, (b) SPC-4, (c) SPC-12, (d) SPC-16, (e) SPC-18, (f) HPW-SPC-4, (g) HPW-SPC-12, (h) HPW-SPC-16, (i) HPW-SPC-18.

3.2. The characterization of the samples

The results of the XRF analysis of the samples are listed in Table 1. It indicates that the actual content of HPW before reaction in the HPW-SPC-4, HPW-SPC-12, HPW-SPC-16, and HPW-SPC-18 samples is 13.1, 13.5, 13.2, and 14.2 wt.% for the nominal content of 15 wt.%, respectively. In addition, the molar ratio of P to W is estimated to be 1:12 in all the samples, suggesting that the Keggin structure unit is well preserved in the products.

The X-ray diffraction patterns of the calcined MMT, SPC and HPW-SPC samples are shown in Fig. 1. The (0 0 1) reflection indicating the layered structure is observed for all of the products [28]. All of the SPC samples have (0 0 1) reflection (Fig. 1b–e), which is corresponding to the basal spacing of 1.77–4.64 nm {$2d \sin\theta = n\lambda$ (θ is corresponding to the angle, $n = 1$, $\lambda = 0.154$ nm)}. It is very important to note that the molecular length of the surfactants is an important factor in the enlargement of the basal spacing of the samples. On the other hand, the characteristic diffraction peak (0 0 1) of the HPW-SPC samples (Fig. 1f–i) slightly shift to the lower angle scope compared to the corresponding SPC samples (b, f; c, g; d, h; e, i). This implies that HPW has been encapsulated into the silica pillared frameworks of the SPC. The results support the proposed formation mechanism of the HPW-SPC samples. The basal spacing and the gallery height (basal spacing – 0.96, here 0.96 nm is the thickness of the clay layer sheet [29]) of the HPW-SPC samples are summarized in Table 2. The refraction peaks of HPW-SPC samples are corresponding to a basal spacing of 1.98–4.80 nm and the corresponding gallery heights are around 1.02–3.84 nm. With the increase of the molecular length of the surfactant, the refraction shift to a low angle scope and the gallery height is found to increase gradually. This indicates that introducing HPW during the intercalation of surfactant does not destroy the SPC mesoporous lamellar structure.

The wide angle XRD patterns of the HPW, calcined HPW-SPC and MMT samples are presented in Fig. 2. All the HPW-SPC samples show the MMT characteristic peaks, which can be assigned to (1 1 0), (0 2 0), (0 0 4), (1 3 0), (2 0 0), (3 3 0) and (0 6 0)

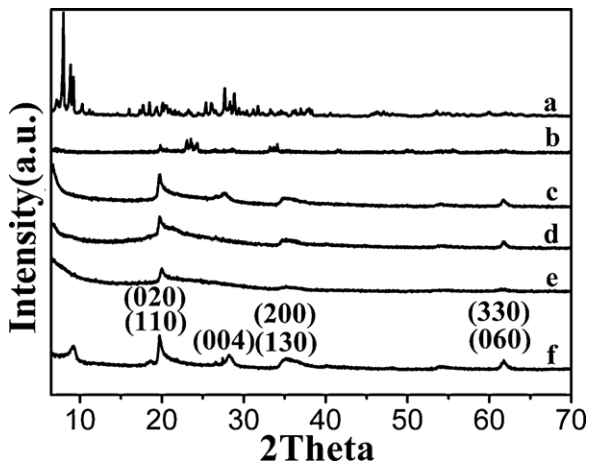

Fig. 2. The wide-angle XRD patterns of the samples: (a) HPW, (b) HPW-SPC-4, (c) HPW-SPC-12, (d) HPW-SPC-16, (e) HPW-SPC-18, and (f) calcined MMT.

diffractions [20,30]. This ulteriorly approves that the laminated structure of MMT and the crystalline structure of the clay sheet have not been destroyed during the intercalation of HPW. However, there are some characteristic peaks of HPW crystal in the pattern of HPW-SPC-4 sample, which indicate that HPW is not highly dispersed in the HPW-SPC-4 samples. This may be due to TBAB caused the relatively small basal spacing, which does not facilitate the incorporation of HPW molecule. For the other samples, the characteristic peaks of HPW can be hardly observed, which illustrates that HPW is highly dispersed in the mesoporous frameworks of the samples.

The TG–DTA curves of the HPW and HPW-SPC samples before calcination in the region of 30–800 °C are shown in Fig. 3. For all the samples, the weight loss below 100 °C is due to the loss of the physisorbed H_2O. For the pure HPW (Fig. 3a), there is an endothermic peak in the temperature range of 100–215 °C (weight loss 2.94%) centered at 206 °C in the DTA diagram, accounting for the loss of 5 H_2O molecules per Keggin unit of the HPW. The broad endothermic peak between 215 and 538 °C centered at about 350 °C is corresponding to the loss of acidic protons and the decomposition of the Keggin structure. The peak centered at 572 °C in the DTA

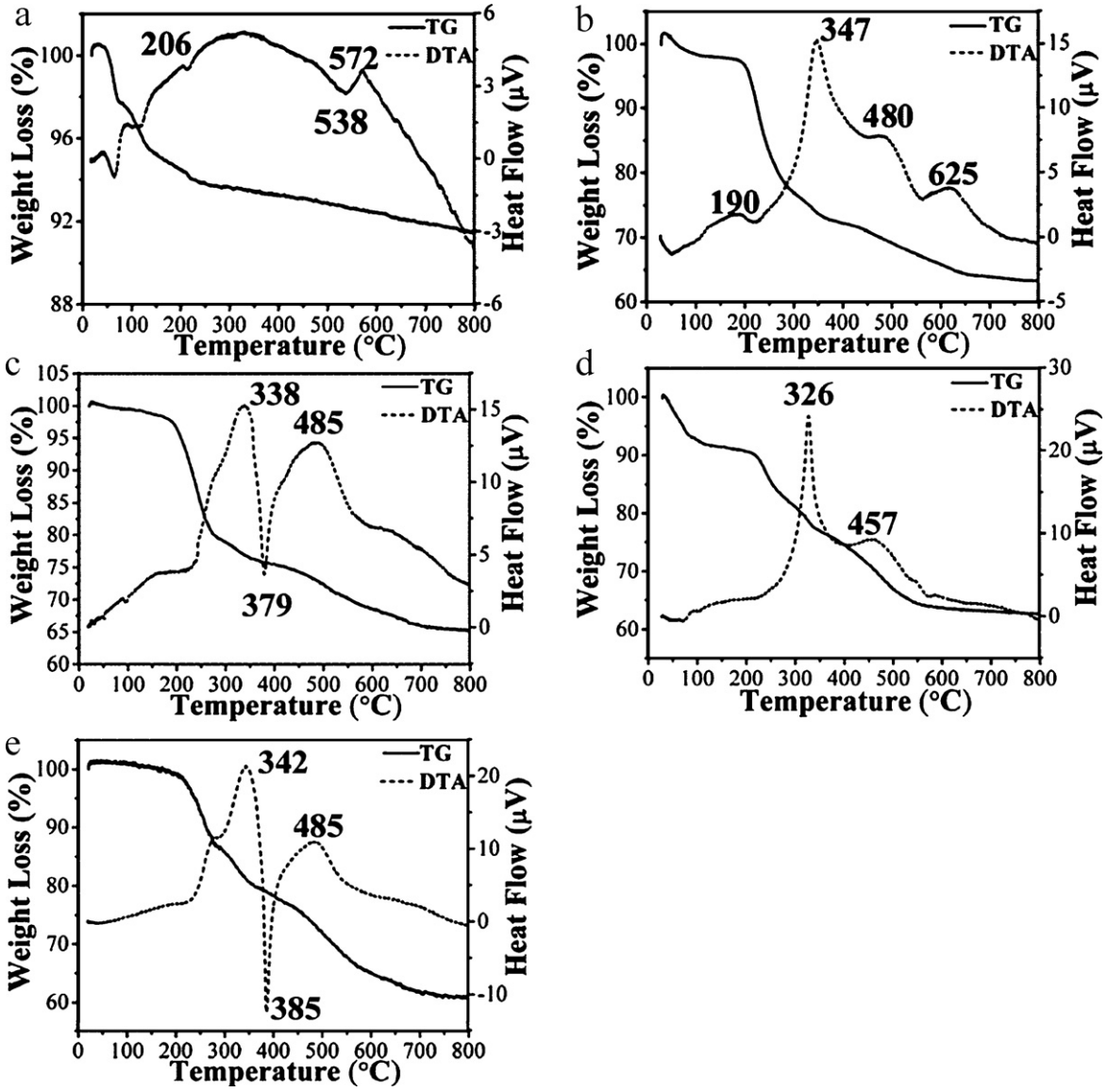

Fig. 3. The TG–DTA curves of the samples: (a) HPW, (b) HPW-SPC-4, (c) HPW-SPC-12, (d) HPW-SPC-16, and (e) HPW-SPC-18.

curve is assigned to the decomposition of heteropoly acid to form mixed oxides [31,32].

For all the HPW-SPC samples, the endothermic peak corresponding to the loss of 5 H_2O molecules per Keggin unit of the HPW also appears at about 200 °C (Fig. 3b–e). The endothermic peaks between 326 and 347 °C in the DTA diagrams can be attributed to the decomposition of surfactants. For the HPW-SPC-12 and HPW-SPC-18 samples, the exothermic peaks accounting for the combustion of the surfactants appear at 379 and 385 °C, respectively. These peaks are evidently stronger than that of the HPW-SPC-4 and HPW-SPC-16 samples, which is due to the heat release of the benzyl in the HPW-SPC-12 and HPW-SPC-18 samples is larger than the alkyl in the other two samples. The endothermic peak accounting for the loss of HPW acidic protons is also evidently observed at 480, 485, 457 and 485 °C in the DTA diagrams of the HPW-SPC-4, HPW-SPC-12, HPW-SPC-16 and HPW-SPC-18 samples, respectively (Fig. 3b–e). Furthermore, the complete decomposition of the heteropoly acid is also evidently observed at 625 °C in the DTA diagram of the HPW-SPC-4 sample (Fig. 3b). And the inconspicuous decomposition peaks in the DTA diagrams of the HPW-SPC-12, HPW-SPC-16 and HPW-SPC-18 samples are also observed at about 650 °C (Fig. 3c–e). The relatively lower decomposition temperature of HPW in the HPW-SPC-4 sample may be due to the agglomeration of HPW molecules on the external surface and the interlayer gallery of the sample, while the HPW has been successfully incorporated into the frameworks of SPC in the HPW-SPC-12, HPW-SPC-16, and HPW-SPC-18 samples. This is in accordance with the results of the XRD. The results indicate that the HPW-SPC samples have enhanced the thermal stability of the HPW heteropoly acid. The TG–DTA curves also show that the HPW-SPC samples can be obtained after treating the solids at 400 °C for 6 h.

The FT-IR spectra of the MMT, pure HPW and HPW-SPC samples in the region of 600–1200 cm^{-1} are shown in Fig. 4. The spectrum of HPW shows a broadened band at 802 cm^{-1}, which is assigned to ν_{as}(W–O_c–W) in edge shared octahedral [33]. In the spectrum of MMT sample, the band at 795 cm^{-1} is attributed to the symmetric stretching frequency of Si–O–Si [34]. In the FT-IR spectra of the HPW-SPC samples, the peak is shifted to 806 cm^{-1}, which is due to the chemical interactions between HPW and SPC. The band can be attributed to the formation of Si–O–W bonds [35]. Therefore, we can conclude that HPW has been encapsulated into the mesoporous silica frameworks and formed new Si–O–W bonds within the silica wall of the SPC material, which is consistent with the proposed formation mechanism of the HPW-SPC samples (Scheme 1). The characteristic bands of Keggin-type HPW are also observed at

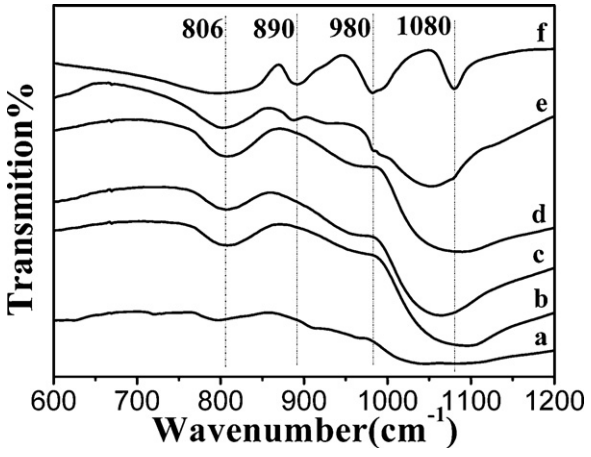

Fig. 4. The FT-IR spectra of the samples: (a) MMT, (b) HPW-SPC-4, (c) HPW-SPC-12, (d) HPW-SPC-16, (e) HPW-SPC-18, and (f) pure HPW.

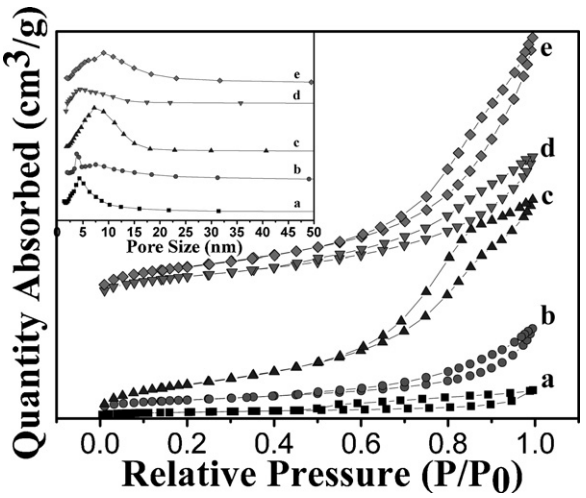

Fig. 5. The N_2 adsorption/desorption isotherms and pore size distribution curves of the samples: (a) MMT, (b) HPW-SPC-4, (c) HPW-SPC-12, (d) HPW-SPC-16, and (e) HPW-SPC-18.

1080, 980 and 890 cm^{-1} (Fig. 4f), which are usually assigned to ν_{as}(P–O), ν_{as}(W=O), and ν_{as}(W–O_b–W) in corner shared octahedral [33], respectively. The band shift at 1080 cm^{-1} in spectra of HPW-SPC-12 and HPW-SPC-18 is due to the large pore sizes formed by the benzyl of the surfactants, which further facilitates the intercalation of the HPW. Thus, the characteristic bands corresponding to the ν_{as}(P–O) is ulteriorly effected by the frameworks of the SPC. The peak of W–O_b–W bond (890 cm^{-1}), however, is hardly observed in the FT-IR spectra for the HPW-SPC-4, HPW-SPC-12 and HPW-SPC-16 samples (Fig. 4b–d), which is due to that the peak is overlapped by the broad and intense peak of Si–O–Si coming from the SPC support. But it can be observed that the peak of the W=O_d (980 cm^{-1}) shifts to a higher wave number in the spectra of HPW-SPC-4, HPW-SPC-12 and HPW-SPC-16 samples, indicating the strong interaction between the Keggin units and the silica matrix [35]. In addition, the bands of the HPW-SPC-18 are evidently strengthened compared to the bands of MMT, which indicates the long carbon chain of surfactant facilitate the incorporation of HPW into the SPC frameworks [36].

The N_2 adsorption/desorption isotherms and the pore size distribution curves of the samples are shown in Fig. 5. The isotherms of the HPW-SPC-12, HPW-SPC-16, and HPW-SPC-18 samples exhibit type IV isotherms (according to IUPAC classification), characteristic of mesoporous materials, and show capillary condensation at higher relative pressures (P/P_0 = 0.4–0.95), while HPW-SPC-4 and MMT samples show isotherms with adsorption at very low relative pressure (P/P_0 < 0.3) and a small hysteresis loop at high relative pressures (P/P_0 = 0.60–0.95), indicating that they possess micropores (Type I) along with small amount of mesopores (Type IV). The isotherms patterns are the characteristic of the materials with the cylindrical pores formed in gallery region [37]. The results of the textural properties of the samples are summarized in Table 2. It is obvious that the pore diameters, S_{BET} and pore volume (V_T) of the HPW-SPC-12, HPW-SPC-16, and HPW-SPC-18 samples are much larger than that of the MMT and HPW-SPC-4 samples. The pore size of the HPW-SPC-4 sample is even smaller than that of the nature MMT. This is due to the HPW-SPC-4 sample cannot form the enough gallery space. When HPW is introduced into the interlayer of the SPC, it will result in pore blockage of the HPW-SPC-4 sample, which in turn decreases its catalytic performance. Furthermore, the desorption branch of the HPW-SPC-4 sample extends to a relatively low pressure, suggesting a partial loss of structural organization and the formation of some narrower slit-shaped pores [26]. Nevertheless, the main part of the hysteresis is still between

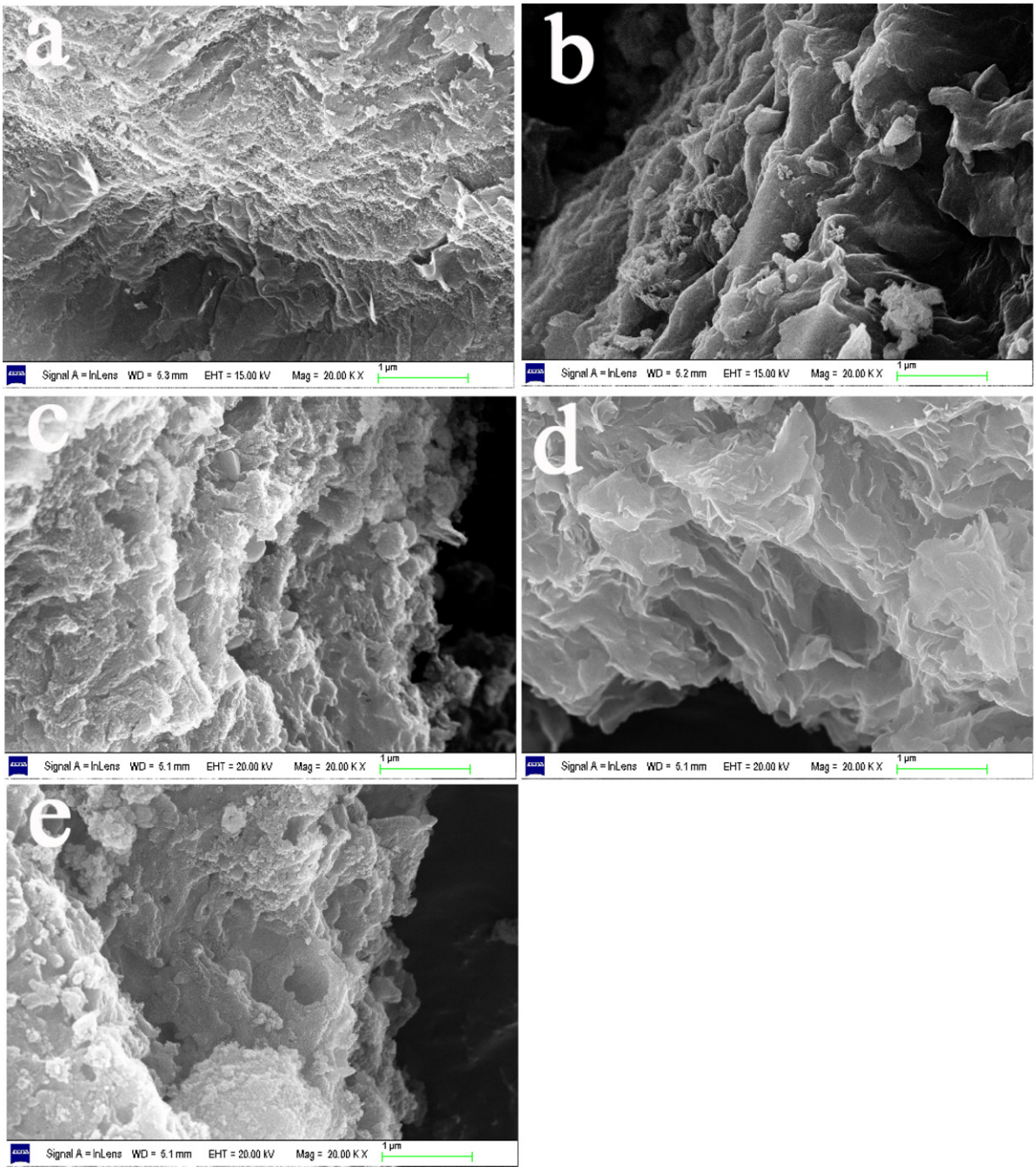

Fig. 6. The SEM images of the samples: (a) MMT, (b) HPW-SPC-4, (c) HPW-SPC-12, (d) HPW-SPC-16, and (e) HPW-SPC-18.

P/P_0 values of 0.60–0.95. It is also obvious that the pore size, S_{BET} and V_T of HPW-SPC-12 and HPW-SPC-18 samples are larger than that of the HPW-SPC-16 samples. The results show that with the increase of the molecular length of the surfactants, the pore size, S_{BET} and V_T of the HPW-SPC samples become larger. In addition, the benzyl molecule can further increase the pore size, S_{BET} and V_T of the materials, which endowed the better catalytic performance of the HPW-SPC-12 and HPW-SPC-18 samples than that of the HPW-SPC-16 sample.

The morphologies of the MMT and HPW-SPC samples are shown in Fig. 6. It is obvious that all the HPW-SPC samples exhibit a slightly swelled nature MMT plates morphology [18], which indicates that the main laminated structure of the samples is retained. The small particles observed around the platelets are probably the broken platelets and the amorphous SiO_2 caused by the hydrolysis of TEOS in the extragallery region of the layered clay. For the HPW-SPC-4 sample, the small particles are also due to the agglomeration of the HPW particles on the surface of the sample. For the HPW-SPC-12 and HPW-SPC-18 samples, the small particles on the surface of the platelets are more than that on the other samples, which show that the benzyl of surfactant has a significant impact in the formation of the interlayer gallery structure of the HPW-SPC-12 and HPW-SPC-18 samples during the incorporation of HPW. These small particles reflect the partial destruction of SPC gallery structure, which may lead to the instability of the samples. However, for the HPW-SPC-16 sample, the laminated structure of the samples is well preserved probably because the HPW has been well encapsulated into the framework of the samples. [38].

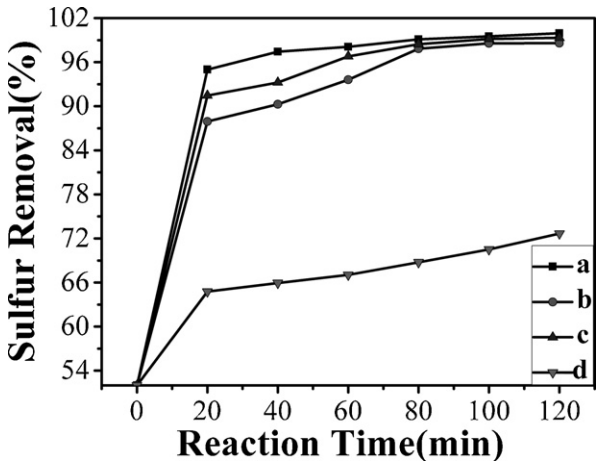

Fig. 7. The effect of the reaction time on ODS over the samples: (a) HPW-SPC-12, (b) HPW-SPC-16, (c) HPW-SPC-18, and (d) HPW-SPC-4.

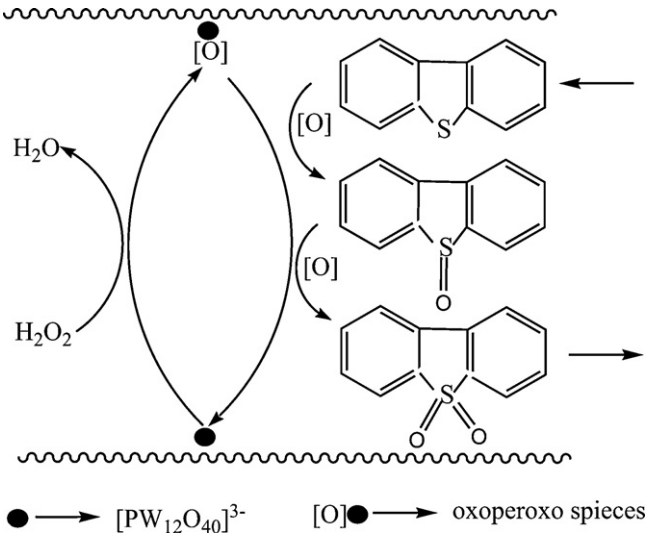

Scheme 2. The proposed reaction mechanism of DBT oxidation.

3.3. Catalytic performance for oxidizing model oil

The effect of the reaction time on ODS of the model oil (500 ppm S) over the HPW-SPC catalysts is shown in Fig. 7. The sulfur removal can reach up to 99.9%, 98.6%, 99.2% and 72.7% within 120 min on HPW-SPC-12, HPW-SPC-16, HPW-SPC-18 and HPW-SPC-4 samples, respectively. The results indicate that the HPW-SPC samples except the HPW-SPC-4 sample are highly efficient in the ODS of DBT. The sulfur removal is not so satisfying on the HPW-SPC-4 sample (Fig. 7d), which is due to that HPW blocked the surface and the interlayer gallery of the SPC leading to the decrease of the S_{BET} and pore size of the HPW-SPC-4 sample (Table 2). The sulfur removal on the HPW-SPC-12 and HPW-SPC-18 catalysts is higher than that on the HPW-SPC-16 catalyst, which is due to the large S_{BET} and pore size of the HPW-SPC-12 and HPW-SPC-18 samples caused by the benzyl group (Table 2).

In order to examine the adsorption capacity for DBT of the catalysts, the tests without adding H_2O_2 and extraction were carried out and the results are shown in Table 3. It is evident that the adsorption capacity for DBT of the catalysts has no distinct difference as compared with the oxidation and extraction, which shows that the MMT and HPW-SPC samples cannot remove DBT effectively just by the adsorption and the best removal of DBT achieves merely 20.3% within 120 min on HPW-SPC-18 catalyst. However, the adsorption capacity for DBT increases slightly with the increase of length of the surfactant. This indicates that the long surfactant facilitates enlarging the pore size, S_{BET} and V_T of the HPW-SPC samples (Table 2), which conduces to the adsorption of DBT. Also, we can see that the HPW-SPC-16 sample showed higher adsorption of DBT than the HPW-SPC-12 sample. This is due to that the HPW-SPC-16 sample has a higher gallery height, which also has an important influence on adsorption of the DBT.

The reusability of HPW-SPC catalysts was investigated in ODS of the model oil. After each catalytic run, the catalysts were recovered by simple filtration, washing with methanol several times, and drying at 110 °C. The results were given in Table 3. It is shown that the catalytic performance of the HPW-SPC-16 sample has no significant decrease after four runs, which is better than that of the HPW-SPC-12 and HPW-SPC-18 samples. According to the previous works [39–42], the Venturello complex $[PW_4O_{24}]^{3-}$ anion forms in these cases in the presence of H_2O_2. And the $[PW_4O_{24}]^{3-}$ anion is the real active species in the oxidation reaction. $[PW_4O_{24}]^{3-}$ anions are stable in solution and the overall structure is conserved in aqueous as well as in organic solvents [43]. In addition, we have measured the chemical content of P and W in the samples by XRF after four times recycle, which are shown in Table 1. From Table 1, we can see that the molar ratio of P:W approximated to be 1:12 in the HPW-SPC-12, HPW-SPC-16, and HPW-SPC-18 samples before and after the reaction, which shows the HPW is stable to some extent. However, the HPW content of the samples decreased after the reaction. The decrease of the HPW content of the samples may be due to the loss of the $[PW_4O_{24}]^{3-}$ and $[WO_4]^{2-}$ anions formed during the reactions. The HPW-SPC-16 sample retained 8.59 wt.% of the HPW, which is higher than that of the HPW-SPC-12 (6.66%) and HPW-SPC-18 (4.75%) samples. The higher remaining content of HPW in the HPW-SPC-16 sample is due to that the pore size (4.5 nm) formed by the CTAB facilitates the encapsulation of HPW into the frameworks of SPC, which leads to the better stability and slight loss of the active species. On the other hand, though the HPW content decreased to 8.59 wt.% in the HPW-SPC-16 sample, the HPW content is still high enough to catalyze the oxidation reaction of the most of DBT in the model oil, leading to the better reusability of the HPW-SPC-16 sample. However, the reusability of the HPW-SPC-12 and HPW-SPC-18 samples is not so satisfying. This may be due to the large pore sizes formed by the benzyl of the surfactants lead to the loss of the active species from the HPW-SPC-12 and HPW-SPC-18 catalysts.

A simplified oxidizing process of DBT is shown in Scheme 2. In the process, HPW accepts active oxygen from the oxidant H_2O_2 to form an oxoperoxo species, which will first oxidize DBT to intermediate dibenzothiophene sulfoxide (DBTO), and then the DBTO was further oxidized to dibenzothiophene sulfone ($DBTO_2$). So the main oxidized products of DBT might be $DBTO_2$ and DBTO. However, the GC–MS analysis (Fig. 8) indicates that there is only $DBTO_2$ and no DBTO is detected in the oxidation products. This confirms that the intermediate product DBTO is quickly transformed to $DBTO_2$. $DBTO_2$ can be extracted by acetonitrile easily and the oil desulfurization is achieved.

Table 3
The results of the catalytic performances of the catalyst (reaction time, 120 min).

Samples	Adsorption	Reusability for ODS			
		1	2	3	4
	Removal/%	Removal/%	Removal/%	Removal/%	Removal/%
MMT	11.2	65.2	–	–	–
HPW-SPC-4	11.9	72.7	–	–	–
HPW-SPC-12	14.6	99.9	99.2	85.4	78.8
HPW-SPC-16	17.2	98.6	98.2	97.8	97.2
HPW-SPC-18	20.3	99.2	81.2	79.4	72.7

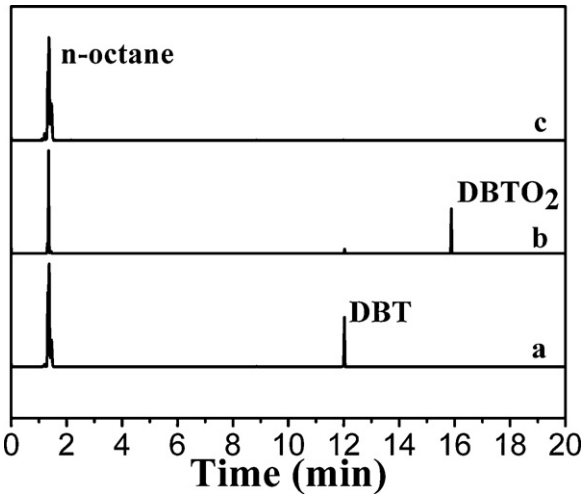

Fig. 8. The GC analysis results of the model oil before and after oxidation. (a) Model oil with DBT content of 500 ppm, (b) model oil after oxidation, and (c) model oil after oxidation and extraction.

4. Conclusions

The mesoporous HPW-SPC materials with various gallery heights and pore sizes were successfully synthesized via hydrolysis of TEOS in the interlayer region of clay in the presence of HPW. The results show that HPW can be encapsulated into the gallery silica frameworks of the HPW-SPC samples, and the surfactants play a decisive role in introducing the HPW molecule. The long surfactants facilitate the enlargement of the interlayer height and pore size of the HPW-SPC samples. Furthermore, the benzyl of the surfactants has a significant impact in the formation of larger pore size and S_{BET}, leading to the better catalytic performance of the HPW-SPC materials. Under the best experimental conditions, DBT can be effectively removed from the model oil by using the HPW-SPC catalysts. The prepared well-organized mesoporous HPW-SPC materials are promising and efficient catalysts for ODS of fuel oils.

Acknowledgements

The work was financially supported by the National Basic Research Program of China (973 Program, Grant No. 2011CBA00506) and State Key Laboratory of Chemical Resource Engineering.

References

[1] R.T. Yang, A.J. Hernández-Maldonado, F.H. Yang, Science 301 (2003) 79–81.
[2] H. Tao, T. Nakazato, S. Sato, Fuel 88 (2009) 1961–1969.
[3] I.V. Babich, J.A. Moulijn, Fuel 82 (2003) 607–631.
[4] E. Ito, J.A. Rob van Veen, Catal. Today 116 (2006) 446–460.
[5] C. Song, X. Ma, Appl. Catal. B: Environ. 41 (2003) 207–238.
[6] A. Anisimov, A. Tarakanova, Russ. J. Gen. Chem. 79 (2009) 1264–1273.
[7] J.M. Campos-Martin, M.C. Capel-Sanchez, P. Perez-Presas, J.L.G. Fierro, J. Chem. Technol. Biotechnol. 85 (2010) 879–890.
[8] C. Hu, M. Hashimoto, T. Okuhara, M. Misono, J. Catal. 143 (1993) 437–448.
[9] H. Lü, J. Gao, Z. Jiang, F. Jing, Y. Yang, G. Wang, C. Li, J. Catal. 239 (2006) 369–375.
[10] L. Yang, J. Li, X. Yuan, J. Shen, Y. Qi, J. Mol. Catal. A: Chem. 262 (2007) 114–118.
[11] H. Ishida, S. Campbell, J. Blackwell, Chem. Mater. 12 (2000) 1260–1267.
[12] R.A. Horch, T.D. Golden, N.A. D'Souza, L. Riester, Chem. Mater. 14 (2002) 3531–3538.
[13] H.Y. Zhu, J.C. Zhao, J.W. Liu, X.Z. Yang, Y.N. Shen, Chem. Mater. 18 (2006) 3993–4001.
[14] Z.E.A. Abdalla, B.S. Li, A. Tufail, Colloids Surf. A: Physicochem. Eng. Aspects 341 (2009) 86–92.
[15] H.H. Mao, B.S. Li, X. Li, Z.X. Liu, W. Ma, Appl. Surf. Sci. 255 (2009) 4787–4791.
[16] L. Chmielarz, B. Gil, P. Kuśtrowski, Z. Piwowarska, B. Dudek, M. Michalik, J. Solid State Chem. 182 (2009) 1094–1104.
[17] P. Cool, E.F. Vansant, Pillared Clays: Preparation, Characterization and Applications, Springer-Verlag, Heidelberg, 1998.
[18] H.H. Mao, B.S. Li, X. Li, Z.X. Liu, W. Ma, Catal. Commun. 10 (2009) 975–980.
[19] H.H. Mao, B.S. Li, X. Li, L.W. Yue, Z.X. Liu, W. Ma, Ind. Eng. Chem. Res. 49 (2010) 583–591.
[20] H.H. Mao, B.S. Li, X. Li, L.W. Yue, Micropor. Mesopor. Mater. 130 (2010) 314–321.
[21] R. Ben Achma, A. Ghorbel, A. Dafinov, F. Medina, Appl. Catal. A: Gen. 349 (2008) 20–28.
[22] C.H. Zhou, X.N. Li, D.S. Tong, Y.F. Zhu, Z.H. Ge, Chin. Chem. Lett. 16 (2005) 261–264.
[23] S. Yoda, Y. Sakurai, A. Endo, T. Miyata, H. Yanagishita, K. Otake, T. Tsuchiya, J. Mater. Chem. 14 (2004) 2763–2767.
[24] B.S. Li, H.H. Mao, X. Li, W. Ma, Z.X. Liu, J. Colloids Interface Sci. 336 (2009) 244–249.
[25] H.H. Mao, B.S. Li, X. Li, Z.X. Liu, W. Ma, Mater. Res. Bull. 44 (2009) 1569–1575.
[26] B.C. Gagea, Y. Lorgouiloux, Y. Altintas, P.A. Jacobs, J.A. Martens, J. Catal. 265 (2009) 99–108.
[27] J.C. Groen, L.A.A. Peffer, J. Perez-Ramirez, Micropor. Mesopor. Mater. 60 (2003) 1–17.
[28] K.W. Park, J.H. Jung, J.D. Kim, S.K. Kim, O.Y. Kwon, Micropor. Mesopor. Mater. 118 (2009) 100–105.
[29] M. Pluta, A. Galeski, M. Alexandre, M.-A. Paul, P. Dubois, J. Appl. Polym. Sci. 86 (2002) 1497–1506.
[30] S. Bracco, P. Valsesia, L. Ferretti, P. Sozzani, M. Mauri, A. Comotti, Micropor. Mesopor. Mater. 107 (2008) 102–107.
[31] I.V. Kozhevnikov, J. Mol. Catal. A: Chem. 262 (2007) 86–92.
[32] S. Ajaikumar, A. Pandurangan, J. Mol. Catal. A: Chem. 286 (2008) 21–30.
[33] C. Rocchiccioli-Deltcheff, M. Foumier, R. Frank, Inorg. Chem. 22 (1983) 207–216.
[34] H.Y. Zhu, Z. Ding, J.C. Barry, J. Phys. Chem. B 106 (2002) 11420–11429.
[35] L.H. Hu, S.F. Ji, Z. Jiang, H.L. Song, P.Y. Wu, Q.Q. Liu, J. Phys. Chem. C 111 (2007) 15173–15184.
[36] A. Bordoloi, F. Lefebvre, S.B. Halligudi, J. Catal. 247 (2007) 166–175.
[37] F. Rojas, I. Kornhauser, C. Felipe, J.M. Esparza, S. Cordero, A. Dominguez, J.L. Riccardo, Phys. Chem. Chem. Phys. 4 (2002) 2346–2355.
[38] J. Ahenach, P. Cool, E.F. Vansant, Phys. Chem. Chem. Phys. 2 (2000) 5750–5755.
[39] D.C. Duncan, R.C. Chambers, E. Hecht, C.L. Hill, J. Am. Chem. Soc. 117 (1995) 681–691.
[40] Y. Matoba, H. Inoue, J. Akagi, T. Okabayashi, Y. Ishii, M. Ogawa, Synth. Commun. 14 (1984) 865–873.
[41] G.D. Yadav, D.V. Satoskar, J. Am. Oil Chem. Soc. 74 (1997) 397–497.
[42] C. Venturello, R. D'Aloisio, J. Org. Chem. 53 (1988) 1553–1557.
[43] L. Salles, C. Aubry, R. Thouvenot, F. Robert, C. Doremieux-Morin, G. Chottard, H. Ledon, Y. Jeannin, J. Bregeault, Inorg. Chem. 33 (1994) 871–878.